AIAA 2001-0664

Predicting the Rotor-Stator Interaction Acoustics of a Ducted Fan Engine

Robert T. Biedron
Christopher L. Rumsey

NASA Langley Research Center, Hampton, Virginia

Gary G. Podboy

NASA Glenn Research Center, Cleveland, OH

M. H. Dunn

Old Dominion University, Norfolk, Virginia

39th AIAA Aerospace Sciences Meeting & Exhibit

8-11 January 2001/Reno, NV

For permission to copy or republish, contact the American Institute of Aeronautics and Astronautics 1801 Alexander Bell Drive, Suite 500, Reston, VA 20191-4344

AIAA-2001-0664

PREDICTING THE ROTOR-STATOR INTERACTION ACOUSTICS OF A DUCTED FAN ENGINE

Robert T. Biedron* and Christopher L. Rumsey†
NASA Langley Research Center
Hampton, Virginia

Gary G. Podboy‡
NASA Glenn Research Center
Cleveland, OH

M. H. Dunn§
Old Dominion University
Norfolk, Virginia

Abstract

A Navier-Stokes computation is performed for a ducted-fan configuration with the goal of predicting rotor-stator noise generation without having to resort to heuristic modeling. The calculated pressure field in the inlet region is decomposed into classical infinite-duct modes, which are then used in either a hybrid finite-element/Kirchhoff surface method or boundary integral equation method to calculate the far field noise. Comparisons with experimental data are presented, including rotor wake surveys and far field sound pressure levels for 2 blade passage frequency (BPF) tones.

1 Introduction

Tone noise in ducted fan engines, resulting from the interaction and response of the moving rotor-blade wakes with the stationary stator vanes, propagates both forward and aft through the duct and radiates to the far field. This noise impacts both communities as well as passengers and crew flying in aircraft. Theoretical models for predicting rotor-stator interaction modes have existed for quite some time (see, e.g., Tyler and Sofrin[1]), but most computational techniques to date rely extensively on experimental measurements and analytical scaling techniques. Although such heuristic methods can provide reasonable predictions of engine tone noise in many cases, they are far from perfect and it is difficult to know where to turn when they are in error. On the other hand, predictions from first principles, although more expensive, hold the promise of offering greater insight into and control of the physical mechanisms behind the noise generation and propagation processes. As computers continue to become more powerful and inexpensive, the greater expense of the first-principles approach is becoming less of an impediment.

Rumsey et al.[2] first explored the use of the first-principles approach for predicting the one blade passage frequency (1 BPF) modes in an advanced ducted propeller (ADP) model. Only the forward-propagating modes were considered. The Navier-Stokes equations were solved time-accurately on a moving grid with sliding patched interfaces between the rotor and stator grids. Turbulent flow was achieved through the use of a one-equation turbulence model with a wall function approach. The acoustic modes inside the engine were both generated and propagated using this numerical method, and a particular mode of interest was shown to propagate well upstream of the rotor inside the engine with minimal attenuation. Separate acoustic codes were used to propagate these internal results out to the far field.

The study of Rumsey et al. demonstrated the

*Research Scientist, Computational Modeling and Simulation Branch.

†Senior Research Scientist, Computational Modeling and Simulation Branch. Associate Fellow AIAA.

‡Aerospace Engineer, Acoustics Branch, Senior Member AIAA.

§Assistant Professor, Department of Mathematics and Statistics, Member AIAA.

Copyright ©2001 by the American Institute of Aeronautics and Astronautics, Inc. No copyright is asserted in the United States under Title 17, U.S. Code. The U.S. Government has a royalty-free license to exercise all rights under the copyright claimed herein for government purposes. All other rights are reserved by the copyright owner.

feasibility of using a Navier-Stokes CFD code to both generate and propagate the tone noise within a ducted fan engine. However, the initial study was for 1 BPF modes, which are often stronger and hence easier to predict than higher harmonic modes. Also, most engines are designed with blade counts such that all 1 BPF modes are cut off (do not propagate), so in this sense the earlier ADP case was unrealistic.

The current study applies the same methodology as Ref. 2 to a more realistic case for which the 1 BPF modes do not propagate but the 2 BPF modes do. Furthermore, more extensive experimental data is available for this new case, including rotor wake velocity profiles between the rotor and stator rows, allowing for a better assessment of the first-principles method. This report details the progress and lessons learned to date, with the purpose of guiding future computational efforts in this area. Specifically, rotor wake profiles between the rotor and stator rows are compared with measured data, and forward-moving acoustic mode amplitudes within the duct are analyzed. These in-duct acoustic results are then used to compute the far field noise in comparison with experimentally measured levels, using both a wave envelope/Kirchhoff method and a boundary integral equation method.

2 Numerical Methods

2.1 Navier-Stokes method in interaction region

The CFD code used in the current investigation is CFL3D,[3] a widely-used structured-grid upwind finite-volume method. It neglects viscous cross-derivative terms, which results in the thin-layer Navier-Stokes equations in specified coordinate directions. Third-order upwind-biased spatial differencing on the convective and pressure terms, and second-order differencing on the viscous terms are used; it is globally second-order spatially accurate. The CFL3D code can solve flow over multiple-zone grids that are connected in a one-to-one, patched, or overset manner, and can employ grid sequencing, multi-grid, and local time stepping when accelerating convergence to steady state. Upwind-biased spatial differencing is used for the inviscid terms, and flux limiting is used to obtain smooth solutions in the vicinity of shock waves, when present. No limiter was employed for this study. Viscous terms are centrally differenced. The flux difference-splitting (FDS) method of Roe is employed to obtain fluxes at the cell faces.

The CFL3D code is advanced in time with an implicit three-factor approximate factorization method. The implicit derivatives are written as spatially first-order accurate, which results in block-tridiagonal inversions for each sweep. However, for solutions that use FDS the block-tridiagonal inversions are further simplified with a diagonal algorithm. Turbulence equations are solved uncoupled from the mean equations.

The turbulence model used is the one-equation Spalart-Allmaras (SA) model,[4] in combination with a wall function approach. The wall function approach obtains a "pseudo"-wall viscosity that forces the law-of-the wall to hold. Details can be found in Ref. 3. The advantage of using the wall function form is that the grid spacing does not need to be as tight near the solid walls ($y^+ \approx 80$ as opposed to $y^+ \approx 1$), so the stretching into the field is less severe. This is particularly important for acoustic computations, for which good grid resolution is needed throughout the field to resolve the acoustic perturbations.

A sliding patched interface connects the rotor and stator rows. At this interface, non-conservative interpolations are used, as described in Rumsey.[5] In this reference, an engineering rule-of-thumb was developed for determining the maximum computational time step allowable so that the acoustic waves that pass through the interface are not distorted. We adhere to this rule-of-thumb in the current work.

For all the computations performed in this study, the CFL3D code was run time-accurately with three τ-TS subiterations per time step performed in combination with multigrid, as described in Refs. 2 and 3.

2.2 Propagation technique to the far field

In principle, the CFD code could be used to directly calculate the far field noise. However, because of the code is only second-order accurate, such an approach would require a prohibitive number of grid points. To make the problem tractable, a hybrid methodology is used that combines the modal data extracted from the CFD solution with more efficient means of computing the far field noise.

Two approaches are considered. In the first, the modal data is input to Eversman's Finite Element Model (FEM) duct radiation code.[6] This velocity-potential based FEM code is then used to propagate the acoustic waves away from the inlet region; no attempt is made to include acoustic propagation from the exhaust flow. While the FEM code has been found to be accurate in the near field, phase information is not well represented in the far field. To overcome this difficulty, a Kirchhoff surface is constructed using the near field FEM solution, and a Kirchhoff integral formulation is employed to com-

pute the noise at any point in the far field. This approach is described in detail in Ref. 7. This was also the approach used in the previous rotor-stator noise study.[2]

The second approach uses the ducted fan noise prediction code TBIEM3D.[8,9] Using boundary integral equation techniques for solving the time harmonic convective wave equation, TBIEM3D calculates the sound scattered by an infinitely thin, constant radius cylindrical duct in a uniform axial flow field. Fan noise generation is approximated by simple spinning monopole or dipole point and/or line sources. In the present simulation, spinning line sources were used to generate the circumferential modes of interest. The line source strengths were adjusted to match as closely as possible the radial mode decomposition from the CFD.

3 Results

3.1 Description of the test case

An advanced high bypass subsonic fan was designed and built by the Allison Engine Company under contract to NASA Glenn Research Center, as described by Woodward et al.[10] The fan has 18 rotor blades with a diameter of 22 in. (0.559 m), and 42 stator vanes. In the acoustic tests performed at NASA Glenn, various configurations of stator vanes were used: forward radial, aft radial, swept only, and swept plus leaned. For the present computations, only the radial stators in the forward position are considered. (In the forward position, the stator leading edge is approximately 3.95 in. (0.10 m) behind the rotor trailing edge.) The computations use a fan speed of 5210 RPM, which is 50% of the nominal design speed (approach setting), and only forward-propagating acoustic modes are considered. The current computations are run using a free stream Mach number of $M = 0.2$. This is higher than the $M = 0.1$ used in Ref. 10. However, the higher free stream Mach number primarily affects the flow external to the engine, including the stagnation point on the cowl. The flow inside the engine itself is primarily determined by the rotor RPM and is not expected to differ significantly for the two conditions. The Reynolds number is taken to be 4.882×10^6 per m.

With 18 rotors and 42 stators, Tyler-Sofrin infinite duct linear theory[1] can be used to determine the forward-moving modes that propagate. Duct acoustic modes are generally characterized as (m, n) modes by their circumferential and radial mode numbers m and n. As discussed in Ref. 1, the mode number m for a rotor-stator interaction can be obtained from $m = hB + kV$, where h is the BPF harmonic, B is the number of rotor blades, V is the number of stator vanes, and k is zero or any positive or negative integer.

In the current study we are focusing on the upstream-moving 2 BPF $m = -6$ modes ($h = 2$ and $k = -1$). All 1 BPF modes are cut-off for this configuration.[11] The $m = -6$ modes are periodic over 1/6th of the engine circumference (60°), and rotate in the direction *opposite* to that of the rotor. These are the lowest-order circumferential modes, and hence have the least stringent grid-spacing requirements for the CFD code; the higher the order the mode, the more points are required to accurately represent it. Given an average in-duct Mach number of $M = 0.265$ between the rotor and stator rows and $M = 0.25$ in front of the rotor, the only $m = -6$ modes that propagate upstream without decay according to the infinite-duct theory are the first three radial modes. The axial wavelengths associated with each of these modes are: $\lambda_{(-6,1)} = 0.087 - 0.089$ m, $\lambda_{(-6,2)} = 0.104 - 0.106$ m, and $\lambda_{(-6,3)} = 0.151 - 0.157$ m. The first number in the range represents the wavelength associated with the higher Mach number. Note that these wavelengths are theoretical values for a constant Mach-number infinite duct; therefore they represent approximate levels expected in the engine, where the Mach number varies.

3.2 Grid size and spacing

For this case, it is necessary to have a grid that covers a full 60° of the inside of the engine. Thus, 3 rotor passages and 7 stator passages must be modeled for the engine with 18 blades and 42 vanes. The grid for the current study is made up of these 10 zones, plus 3 additional zones modeling the exterior of the engine, out to a far field approximately 37 in. (0.95 m) in front, 62 in. (1.57 m) above, and 53 in. (1.35 m) behind the engine cowl (the engine cowl is approximately 34.5 in. (0.88 m) long). An overall view of the far field grid is shown in Fig. 1. The grid size of each rotor passage is $321 \times 57 \times 41$ (these numbers represent axial, radial, and circumferential spacing, respectively). The grid size of each stator passage is $129 \times 57 \times 33$. There are approximately 4.12×10^6 total grid points in the 13 zones.

To do a reasonable job in an engine acoustic computation, the CFD code has to adequately resolve two important aspects of the flow: the "creation" phase and the "propagation" phase. The "creation" phase is the phase that occurs near the stator leading edge, where the interaction of the rotor wakes with the vanes creates the duct acoustic modes in the first place. The "propagation" phase is the advection of these modes through the flow field. The

idea behind a first-principles approach is to use the Navier-Stokes equations to resolve both the creation and propagation phases within the highly nonlinear regime of the engine, where simpler linear acoustic methods are not expected to be valid. Once the acoustic modes have been propagated away from the nonlinear regions, linear acoustic methods can then take over and be used to determine the noise in the far field.

The grid size and spacing is a very crucial aspect of an engine acoustic computation. This point cannot be stressed enough. To apply the current first-principles approach to compute acoustic features, it is necessary to sufficiently resolve the acoustic waves of interest as they propagate *and* the region where the acoustic modes are initially generated must be fine enough to adequately resolve their creation. Several close-ups of the grid are shown in Figs. 2 - 6. The grid was generated using TIGER.[12] In the following paragraphs, we will point out some important elements of the grid and their relationship to the acoustic aspects of the computation.

The grid is clustered near all solid walls, and stretches as it moves into the interior. As mentioned earlier, to avoid cells that are too large (because of too-large stretching factors), we utilize a turbulence model with a wall function and use a minimum spacing near walls such that the y^+ level at the first grid point from the wall averages approximately 80. The current grid maintains fine axial spacing within the engine from the front of the inlet to past the leading edge on the stator. This axial spacing is fine enough so that there are at least 25 - 30 points per axial wavelength for each acoustic mode of interest. The results for the model problem studied in Ref. 5 indicate that this is an adequate resolution, at least for 1 BPF modes. A view of the $k = 1$ planes of one rotor and one stator passage is given in Fig. 2. (Note that the figure distorts the inner cowl apparent shape, because the grid lines sweep circumferentially to align with the rotor angled direction.) The axial spacing is necessarily clustered in the regions near the leading and trailing edges, but the average spacing elsewhere ranges from roughly 0.05 in. (0.0013 m) to 0.12 in. (0.0031 m). Typical circumferential spacing in the rotor and stator zones between the two rows of blades is shown in Fig. 3. Clustering in the circumferential direction is necessary both for the wake region (see below) as well as near the blades.

In front of the engine inlet and behind the stators, the Navier-Stokes code is no longer used to track the acoustic modes, so the grid is allowed to stretch axially in these regions. This stretching accomplishes two objectives: it reduces the total grid size, and it diffuses potential spurious reflections from the exterior boundaries of the grid. (If one were to attempt this type of computation with only an unstretched internal-engine grid, the acoustic field would be contaminated by reflections from the boundary unless special non-reflective acoustic boundary conditions were employed.)

Reasonably accurate resolution of the rotor wakes is necessary, because it is their interaction with the stator vanes that causes the tonal acoustic modes. To achieve high resolution, the rotor grids must be clustered near the approximate location of the wakes as they convect aft. A view of the $j = 35$ planes of one rotor and one stator passage are shown in Fig. 4. The "wake cuts" of the rotor grid are approximately aligned with the local rotor direction, so the grid lines follow the approximate paths of the wakes themselves. Additionally, the rotor grids extend downstream to be within 0.877 in. (0.022 m) of the stator leading edge. As a result, the rotor wakes are in a "clustered-grid" region for a long distance before the wake passes through the rotor-stator interface, where clustering is minimized to improve inter-grid interpolations.

Initial computations with what was originally considered "reasonable" axial spacing near the stator leading edge led to results in which the $(-6, 1)$ mode was not captured at all in the "creation" phase. It was subsequently determined that considerably finer spacing is required near the stator leading edge. A close-up of the stator leading edge region in the current grid is shown in Fig. 5. It is still an open question whether even finer grid spacing in the regions surrounding the leading edge would significantly benefit the prediction of the acoustic modes.

In all of the computations done for this study, the rotor tip gap is crudely modeled by collapsing ("zipping") the rotor grid zones for the upper 5 grid points. This zipping results in an average tip gap spacing of approximately 0.03 in. (7.6×10^{-4} m), which is similar to the actual tip gap measured in the experiment near the leading edge, but is over three times larger than the tip gap measured at the trailing edge. A view of the rotor tip is shown in Fig. 6, looking aft. We originally attempted to model the actual tip gap spacings, but the finer grid spacing required near the trailing edge made grid generation more difficult and also caused excessive local stretching factors that we decided were best to avoid.

3.3 Computations

Computations were performed at a nondimensional time step of $\Delta t' = 0.05$ (nondimensionalized by characteristic length divided by free stream

speed of sound). The characteristic length in the CFD solution is 1 in. (0.0254 m) and the speed of sound is taken as $c_\infty = 340.445$ m/s. Dimensionally, this time step corresponds with a time step of $\Delta t = 3.73 \times 10^{-6}$ s. The frequency of all 2 BPF modes is given by $K = 2B\Omega/c = 57.69$ m^{-1}, so the time corresponding to one period is $t_p = 2\pi/(c_\infty K) = 3.2 \times 10^{-4}$ s. (A given rotor blade rotates through 1 blade passage = 20° in 6.4×10^{-4} s.) Thus, the current time step yields approximately 86 time steps per period for the 2 BPF modes. This number exceeds the 60 recommended in Ref. 5.

As a first phase of the computation for this case, we investigate the ability of the CFD code to propagate a specified duct acoustic mode forward through the duct. We do this by removing the stator grid zones and specifying time-varying duct acoustic pressures at the exit face of the rotor grids, according to the formula:

$$p(r, \theta, x) = A J_m(K_r r) \exp i[c_\infty K t - m\theta - K_a x]. \quad (1)$$

A is the magnitude of the perturbation, J_m is the Bessel function of the first kind and order m, K_r is the radial wave number, and K_a is the axial wave number. In essence, this computation is a check to test whether the grid resolution is sufficiently fine for the *propagation* part of the computation. In other words, given a duct acoustic mode of given strength, is the given grid fine enough to propagate it forward without significant attenuation to the rotor blades (where some of the mode is scattered into different frequencies[13]); and, for the part of the mode that survives the passage through the rotor, is the given grid in front of the rotor fine enough to propagate it forward without significant attenuation to the duct inlet?

As shown in Figs. 7 and 8, when an initial $(-6, 1)$ mode acoustic amplitude of approximately $A = 40$ Pa is imposed at the rear of the rotor grid, it propagates forward to the trailing edge of the rotor blades with very little attenuation on either the fine or medium-level grid. Then, roughly a third of the wave strength makes it through the rotors. The wave is propagated forward on the fine grid all the way to the inlet with no attenuation, whereas on the medium-level grid it loses a small percentage of its strength. Therefore, the current fine grid appears to be fine enough for the *propagation* of the $(-6, 1)$ mode of interest.

Next, we run the full problem, including the stators, and determine the ability of the CFD code to successfully *generate* the 2 BPF modes. As a first step, we compare the computed rotor wakes with LDV data taken at NASA Glenn Research Center. The first station corresponds to the LDV location closest to the rotor while the second station corresponds to the LDV location closest to the stator. The second station is located within the stator zones of the computational grid. Note that the LDV data was taken with the stator vanes in the aft position, whereas the CFD is performed with the stators in the forward position. However, the position of the stators is not expected to significantly impact the rotor wakes at the positions measured. Axial velocity contours at constant axial positions are shown in Figs. 9 - 12, with computed contours corresponding to the fine grid. Generally speaking, the computed wakes are much narrower and exhibit more curvature than the LDV measurements. Axial velocity defect profiles at a radius of approximately 8.5 in. (0.216 m) are shown in Figs. 13 and 14, corresponding to the dashed lines in Figs. 9 - 12. Although the computed width and general shape are different from the experiment, CFD does a reasonable job capturing the depth of the rotor wake as well as the overall trend of its evolution downstream. The axial velocity defects on the fine grid are not much different from the medium grid at the first station, but at the second station the wake depth of the fine grid is larger and in better agreement with experiment.

We now turn to an analysis of the duct acoustic modes generated by the Navier-Stokes code. This is done in a post-processing step by decomposing the instantaneous pressures output by CFL3D within the duct into its component duct mode strengths. The strength A of the $(-6, 1)$ mode is shown between the rotor and stator rows in Fig. 15 and in front of the rotor row in Fig. 16. Axial distances in these figures are given in terms of the distance forward of the rotor stacking axis. The mode strength approaches a quasi-constant level as it propagates forward toward the rotor trailing edge, and is roughly constant after it passes through the rotor row and travels forward through the duct. The wave-like structure is evident in both figures, and is close to the theoretical value of $\lambda_{(-6,1)} \approx 0.09$ m.

Note in Fig. 15 that there is no distortion in the acoustic signal evident near the rotor-stator sliding-zone interface at $x = -0.1256$ m. This lack of distortion indicates successful transfer of acoustic information across the patched interface.[5] Between the rotor and stator rows, the $(-6, 1)$ strength from the fine grid averages roughly 20 Pa, and in front of the rotor row, it averages roughly 5 Pa. This 75% percent reduction in mode strength is similar to that seen in the earlier prescribed-mode case. There is a modest increase in magnitude of the mode strength between the medium and fine level grids in front

of the rotor, indicating that further refinement beyond the fine grid may still yield increased acoustic strength. Results for the $(-6,2)$ and $(-6,3)$ modes in front of the rotor are shown in Figs. 17 and 18. The $(-6,2)$ mode from the fine grid is very weak, with an average strength of only about 3 Pa. The $(-6,3)$ mode has a higher amplitude of about 10 Pa. The wavelengths of both the $(-6,2)$ and $(-6,3)$ modes are close to the theoretical levels. Note that, among the three modes, the $(-6,3)$ mode shows the most significant change in magnitude between the medium and fine level grids.

Although not shown, as a further check on the acoustic computations, we studied the mode behavior at a given station in front of the rotor as a function of time. Given that the mode behavior is kinematically determined, we know theoretically how much it should rotate in a given number of iterations. Results confirm that the $(-6,1)$ and $(-6,3)$ modes rotate at approximately the correct rate and in the correct direction. The $(-6,2)$ mode is too weak to yield meaningful analysis.

4 Far Field Noise

The final step in the current study was to use the extracted $m = -6$ modal strengths in the inlet duct forward of the fan (at $x = 0.1269$ m) to predict the far field noise. The predicted far field directivity is shown in Fig. 19. Note that past approximately 60 deg., the measured levels in the experiment are elevated due to aft-end noise, which was not included in the CFD computation. As can be seen, the computed sound pressure levels forward of 60 deg. are significantly lower than the experimentally measured levels, using both the FEM/Kirchhoff approach and the TBIEM3D approach. (Note that TBIEM3D uses an idealized duct, whereas FEM/Kirchhoff uses the actual duct geometry. Thus, results are not expected to agree; for example, TBIEM3D yields higher SPLs at higher emission angles because of diffraction from the idealized duct's sharp leading edge.) The cause of the discrepancy between CFD and experiment is therefore almost certainly related to the extracted modal data from the CFD solution – the computed source strengths in the inlet region are too low by about a factor of 3–6.

As discussed previously, there is a 65%-75% reduction in the modal amplitudes as the waves generated by rotor-stator interaction travel forward through the rotor and into the inlet. Although not shown, if the transmission losses through the rotor are ignored, i.e., if the modal strengths between the stator and the rotor (e.g., Fig. 15) are used instead of those in front of the rotor (e.g. Fig. 16), then the predicted far field noise levels increase by nearly 10 dB and are much closer to the experimental measurements. Other noise-prediction methodologies ignore the transmission losses entirely.[11]

Why the inlet modal strengths are underpredicted remains an open question. It may be that the interaction of the rotor wakes with the stators is not predicted adequately because the predicted rotor wakes are much narrower than the measured wakes. This underprediction of wake width is possibly due to either inadequate physics in the turbulence model or under-resolution of the rotor wake vortical structure and its inherent unsteadiness.

Thinking in terms of a Fourier transform of the rotor wakes in the circumferential direction, narrower wakes have a higher frequency content than wider wakes. Perhaps, then, the computed noise sources are biased towards harmonics higher than 2 BPF. Alternatively, the losses that occur as the sound propagates forward through the rotors may be exacerbated by the numerical scheme. However, solutions obtained for two grid resolutions did not show a significant variation of the modal amplitudes with mesh size.

5 Summary

Performing acoustic computations on full rotor-stator ducted fan configurations using the Navier-Stokes equations is by no means a simple push-button task. The work presented here is the second of a series of computations performed to assess whether Navier-Stokes solvers can be used to directly capture the sound generation mechanisms of rotor-stator interaction, without resorting to more heuristic modeling techniques. The earlier study, for a configuration exhibiting 1 BPF tones, had a fair degree of success in predicting the far field noise. In the current study, for which the lowest order propagating modes are 2 BPF, the predicted far field noise levels are about 10–12 dB low. It was determined that the *propagation* within the duct of the 2 BPF modes was not as difficult as their *creation* via the first-principles approach. The wake widths obtained from the computation were considerably narrower than those measured in the experiment. This may be be the primary cause of the discrepancy in the computed and measured far field noise levels. Additional research is needed to explore in greater depth the grid and turbulence model requirements in the interaction region where the rotor wakes convect and the acoustic modes are created.

Acknowledgments

The authors would like to thank F. Farassat of NASA Langley Research Center for many fruitful discussions during the course of this work. The authors also thank R. Woodward of NASA Glenn Research Center for providing measured sound data, and L. Heidelberg and D. Huff of NASA Glenn Research Center for their advice and expertise.

References

1. Tyler, J. M. and Sofrin, T. G., "Axial Flow Compressor Noise Studies," SAE Transactions, Vol. 70, 1962, pp. 309–332.

2. Rumsey, C. L., Biedron, R. T., Farassat, F., and Spence, P. L., "Ducted-Fan Engine Acoustic Predictions Using a Navier-Stokes Code," *Journal of Sound and Vibration*, Vol. 213, No. 4, 1998, pp. 643–664.

3. Krist, S. L., Biedron, R. T., and Rumsey, C. L., "CFL3D User's Manual (Version 5.0)", NASA TM-1998-208444, June 1998.

4. Spalart, P. R., and Allmaras, S. R., "A One-Equation Turbulence Model for Aerodynamic Flows," *La Recherche Aerospatiale*, No. 1, 1994, pp. 5–21.

5. Rumsey, C. L., "Computation of Acoustic Waves Through Sliding-Zone Interfaces," *AIAA Journal*, Vol. 35, No. 2, 1997, pp. 263–268.

6. Roy, I. D., Eversman, W., and Meyer, H. D., "Improved Finite Element Modeling of the Turbofan Engine Inlet Radiation Problem," Report Prepared for NASA Lewis Research Center Under Contract NAS3-25952, Task 10, April 1993.

7. Spence, P., "Ducted Fan Noise Prediction Using Wave Envelope Analysis and the Kirchhoff Formula," AIAA Paper 97-1651, May 1997.

8. Dunn, M. H., "TBIEM3D - A Computer Program for Predicting Ducted Fan Engine Noise, Version 1.1," NASA/CR-97-206232, September 1997.

9. Dunn, M. H., Tweed, J., and Farassat, F., "The Application of a Boundary Integral Equation Method to the Prediction of Ducted Fan Engine Noise," *Journal of Sound and Vibration*, Vol. 227, No. 5, 1999, pp. 1019–1048.

10. Woodward, R. P., Elliot, D. M., Hughes, C. E., and Berton, J. J., "Benefits of Swept and Leaned Stators for Fan Noise Reduction," AIAA Paper 99-0479, January 1999.

11. Envia, E., and Nallasamy, N., "Design Selection and Analysis of a Swept and Leaned Stator Concept," NASA TM-1998-208662, December 1998.

12. Shih, M. H., Soni, B. K., and Janus, J. M., "TIGER: Turbomachinery Interactive Grid Generation / Flow Simulation System User's Manual," Mississippi State University Publication, 1994.

13. Hanson, D. B., "Coupled Two-Dimensional Cascade Theory for Noise and Unsteady Aerodynamics of Blade Row Interactions in Turbofans," NASA CR-4506, 1994.

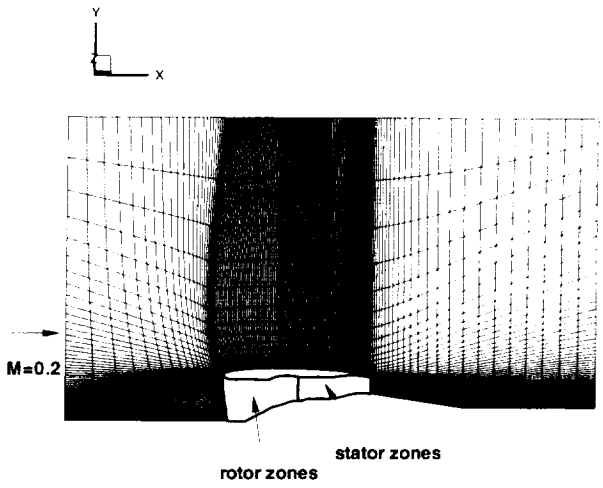

Figure 1. Far field view of grid ($k = 1$ plane).

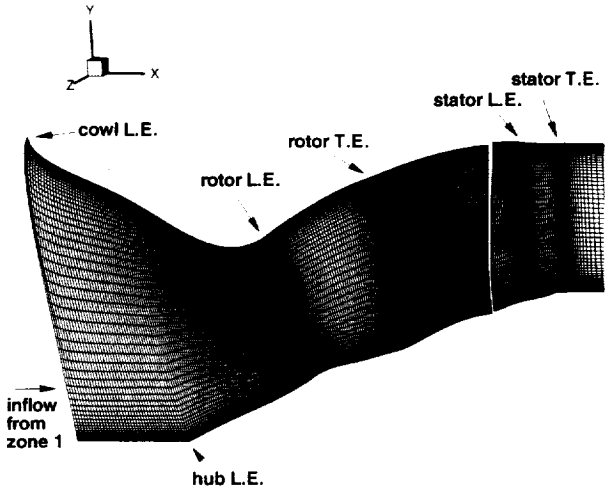

Figure 2. View of rotor and stator grid zones ($k = 1$ plane).

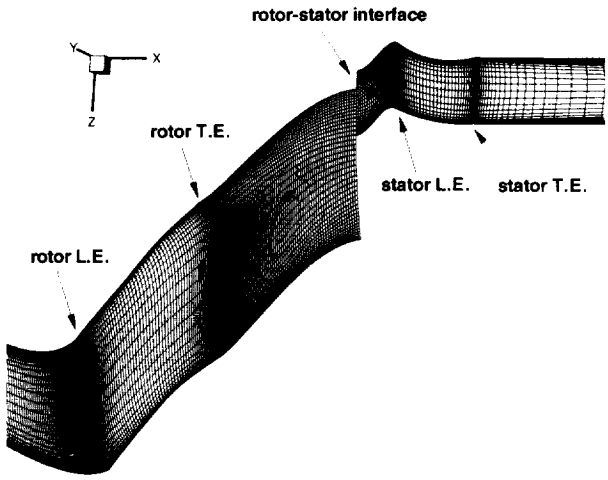

Figure 4. View of rotor and stator grid zones ($j = 35$ plane).

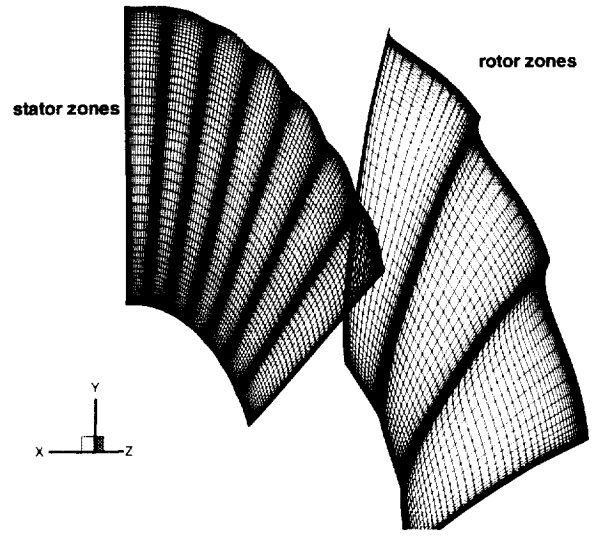

Figure 3. View of rotor and stator grid zones ($i = 250$ plane in rotor zones and $i = 19$ plane in stator zones).

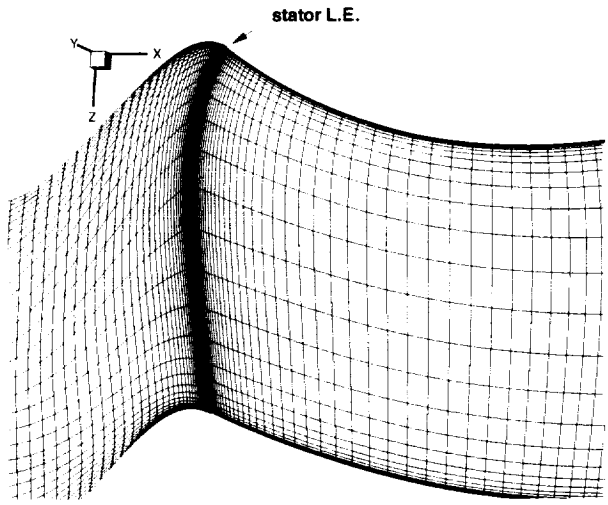

Figure 5. Close-up view near stator leading edge ($j = 35$ plane).

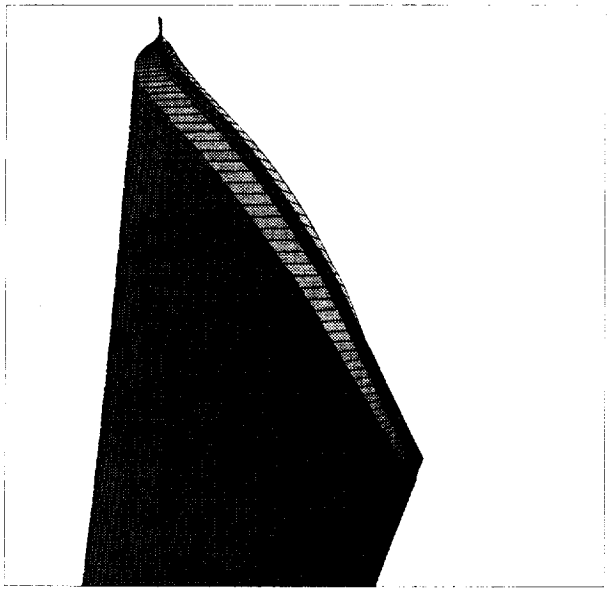

Figure 6. Close-up view of rotor tip region.

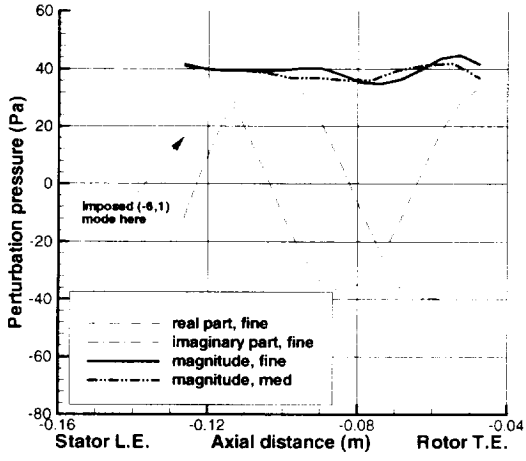

Figure 7. Strength of forward-moving imposed $(-6, 1)$ mode between imposed location and rotor trailing edge.

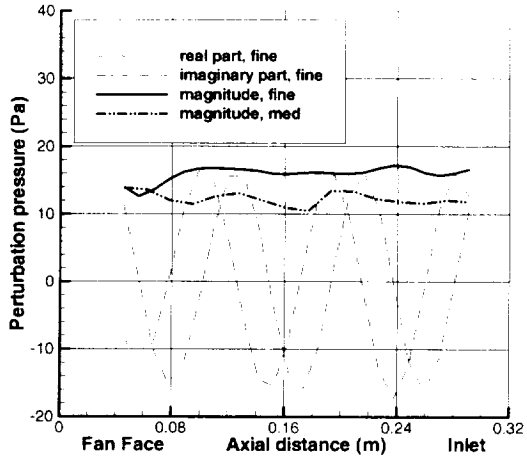

Figure 8. Strength of forward-moving imposed $(-6, 1)$ mode in front of rotor row.

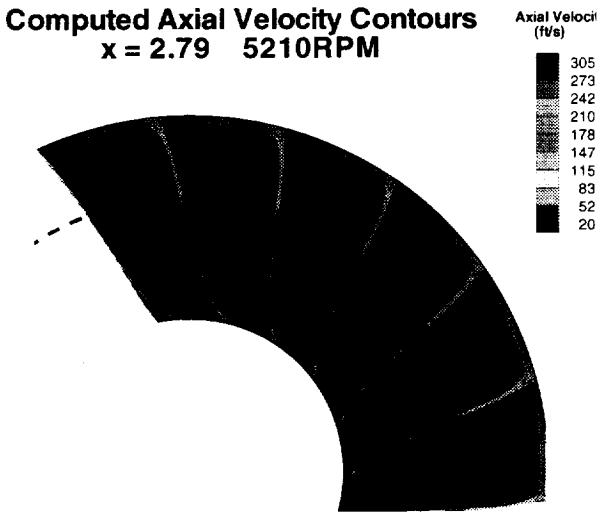

Figure 9. Computed axial velocity contours 1.2 in. (0.030 m) downstream of rotor tip trailing edge, within rotor zones; dashed lines show location for wake defect plots.

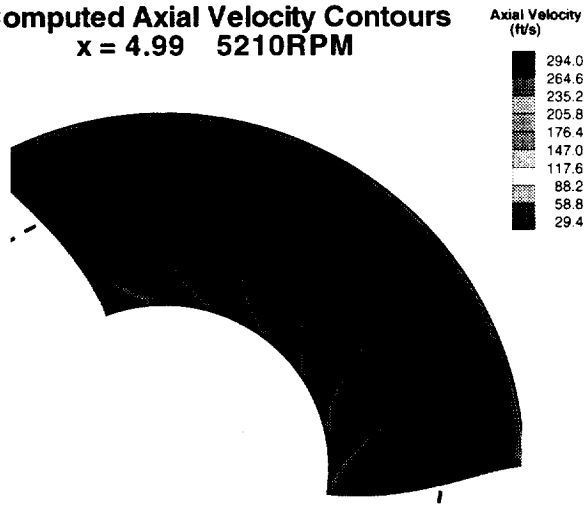

Figure 11. Computed axial velocity contours 3.4 in. (0.086 m) downstream of rotor tip trailing edge, within stator zones; dashed lines show location for wake defect plots.

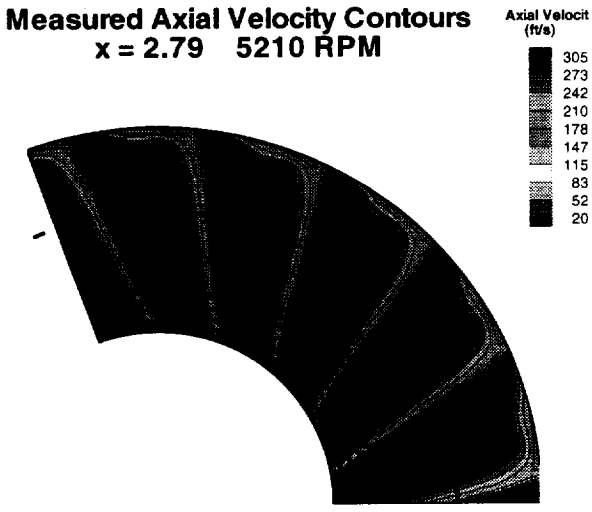

Figure 10. Measured axial velocity contours 1.2 in. (0.030 m) downstream of rotor tip trailing edge, within rotor zones; dashed lines show location for wake defect plots.

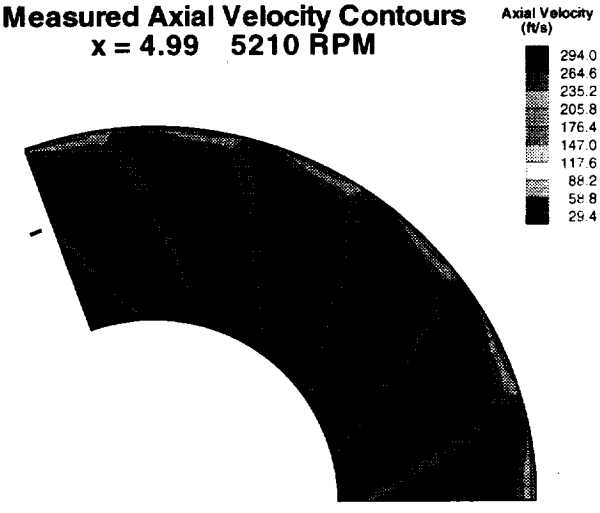

Figure 12. Measured axial velocity contours 3.4 in. (0.086 m) downstream of rotor tip trailing edge, within stator zones; dashed lines show location for wake defect plots.

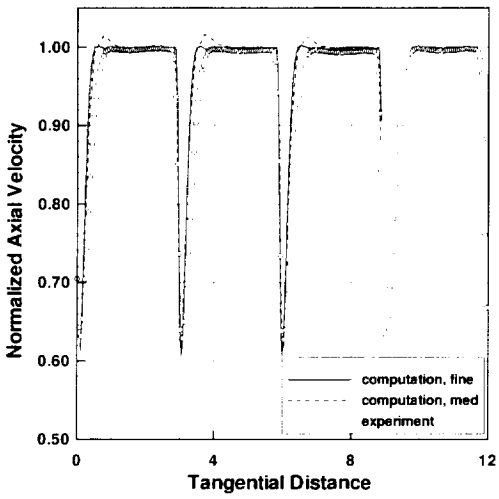

Figure 13. Normalized axial velocity defect 1.2 in. (0.030 m) downstream of rotor tip trailing edge, within rotor zones, at radius near 8.5 in. (0.216 m).

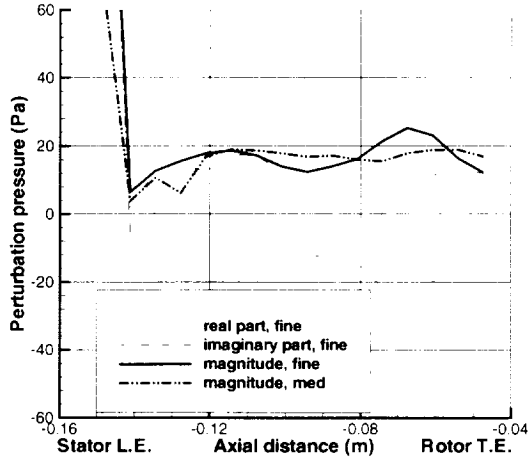

Figure 15. Strength of forward-moving computed $(-6, 1)$ mode between the stator row and rotor row.

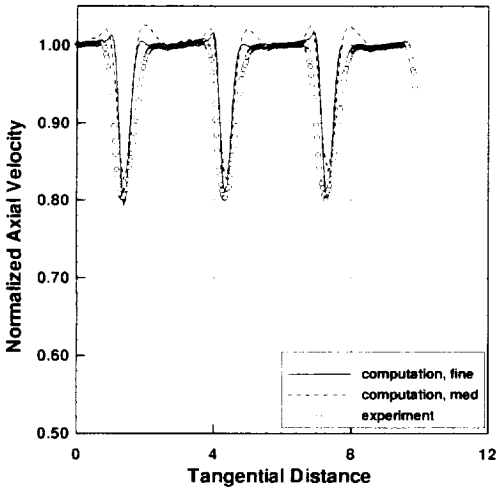

Figure 14. Normalized axial velocity defect 3.4 in. (0.086 m) downstream of rotor tip trailing edge, within stator zones, at radius near 8.5 in. (0.216 m).

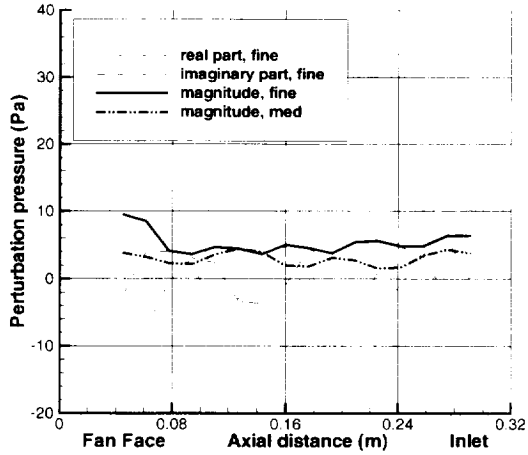

Figure 16. Strength of forward-moving computed $(-6, 1)$ mode in front of the rotor row.

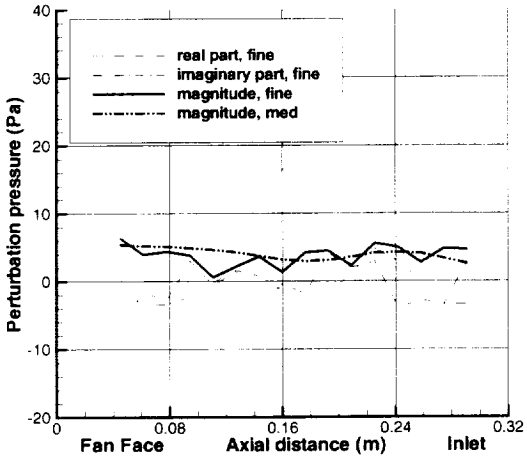

Figure 17. Strength of forward-moving computed $(-6, 2)$ mode in front of the rotor row.

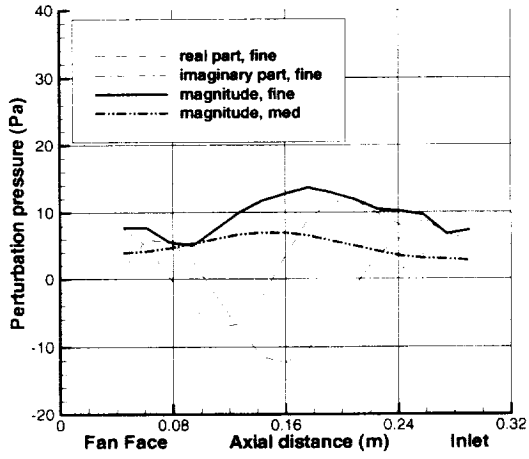

Figure 18. Strength of forward-moving computed $(-6, 3)$ mode in front of the rotor row.

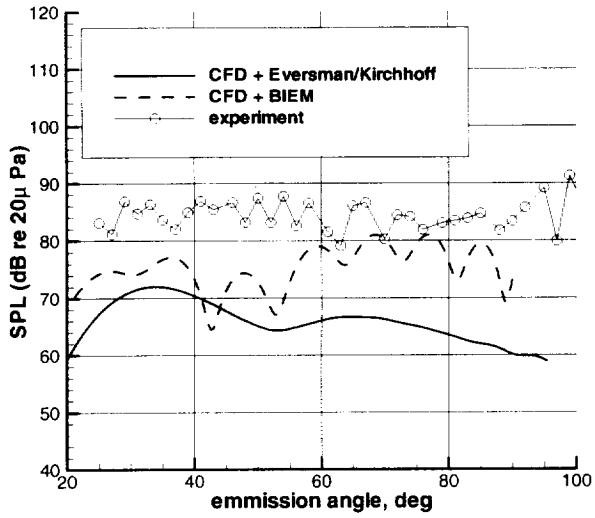

Figure 19. Far field sound pressure levels; narrowband directivities for 2 BPF tone along a 2.24 m (88 in.) sideline, $M_\infty = 0.1$.